# Methane production related to microbiota in dairy cattle feces

Jian Liu, Meng Zhou, Lifeng Zhou, Run Dang, Leilei Xiao, Yang Tan, Meng Li, Jiafeng Yu, Peng Zhang, Marcela Hernández, et al.

Environmental Research 267 (2025) 120642
https://doi.org/10.1016/j.envres.2024.120642

# Methane production related to microbiota in dairy cattle feces

Jian Liu [a,d], Meng Zhou [b,*], Lifeng Zhou [c,e], Run Dang [c,e], Leilei Xiao [c], Yang Tan [c], Meng Li [a,d], Jiafeng Yu [a,d,**], Peng Zhang [f], Marcela Hernández [g], Eric Lichtfouse [h]

[a] Shandong Key Laboratory of Biophysics, Institute of Biophysics, Dezhou University, Dezhou, 253023, China
[b] State Key Laboratory of Black Soils Conservation and Utilization, Northeast Institute of Geography and Agroecology, Chinese Academy of Sciences, Harbin, 150081, China
[c] CAS Key Laboratory of Coastal Environmental Processes and Ecological Remediation, Yantai Institute of Coastal Zone Research, Chinese Academy of Sciences, Yantai, 264003, China
[d] International Joint Laboratory of Agricultural Food Science and Technology of Universities of Shandong, Dezhou University, Dezhou, 253023, China
[e] Liaocheng University School of Geography and Environment, Liaocheng, 252059, China
[f] Faculty of Environmental Science & Engineering, Kunming University of Science & Technology, Kunming, 650500, Yunnan, China
[g] School of Biological Sciences, University of East Anglia, Norwich, NR4 7TJ, UK
[h] State Key Laboratory of Multiphase Flow in Power Engineering, Xi'an Jiaotong University, Xi'an, 710049, Shaanxi, China

Methane ($CH_4$) emission from livestock feces, led by ruminants, shows a profound impact on global warming. Despite this, we have almost no information on the syntrophy of the intact microbiome metabolisms, from carbohydrates to the one-carbon units, covering multiple stages of ruminant development. In this study, syntrophic effects of polysaccharide degradation and acetate-producing bacteria, and methanogenic archaea were revealed through metagenome-assembled genomes from water saturated dairy cattle feces. Although $CH_4$ is thought to be produced by archaea, more edges, nodes, and balanced interaction types revealed by network analysis provided a closed bacteria-archaea network. The $CH_4$ production potential and pathways were further evaluated through dynamic, thermodynamic and $^{13}C$ stable isotope analysis. The powerful $CH_4$ production potential benefited from the metabolic flux: classical polysaccharides, soluble sugar (glucose, galactose, lactose), acetate, and $CH_4$ produced via typical acetoclastic methanogenesis. In comparison, a cooperative model dominated by hydrogenotrophic methanogenic archaea presented a weak ability to generate $CH_4$. Our findings comprehensively link carbon and $CH_4$ metabolism paradigm to specific microbial lineages which are shaped related to developmental stages of the dairy cattle, directing influencing global warming from livestock and waste treatment.

## 1. Introduction

Climate warming is a global problem of great concern but difficult to contain. In a global context, farm animals exacerbate greenhouse gas emissions via ruminants, manure, and land use to meet increasing global food demand (Boetius, 2019). Livestock has became the second-largest anthropogenic contributor to the global $CH_4$ budget, contributing to nearly one-fifth of total emissions (Chang et al., 2019; Mizrahi et al., 2021; Saunois et al., 2016). Based on data from the Food and Agriculture Organization (FAO) on $CH_4$ emission in 2019, India, Brazil, China, and the United States of America are the top four $CH_4$ emitters, each exceeding 6 Tg/a (Fig. S1a). Cattle (non-dairy and dairy), buffaloes, goats, and sheep are recognized as the main livestock types, together representing 96% of the global enteric fermentation source for $CH_4$ emission, with a total of more than 100 Tg in 2019 (Fig. S1).

Livestock waste is considered an important breeding ground for $CH_4$ production (Hou et al., 2017; Owen and Silver, 2015). Steady attention on $CH_4$ emission from biowaste of livestock is proposed, suggesting its deterioration on the global climate (Bhattacharya et al., 1997; Hou et al., 2015). Most developing regions, such as Asia, Latin America, and Africa, have experienced a significant increase in emissions since 1961 (Dangal et al., 2017). Studies also highlight the geographical distribution and

* Corresponding author. State Key Laboratory of Black Soils Conservation and Utilization, Northeast Institute of Geography and Agroecology, Chinese Academy of Sciences, No. 138 Haping Rd., Harbin, 150081, China.
** Corresponding author. Shandong Key Laboratory of Biophysics, Institute of Biophysics, Dezhou University, No. 566 University Rd. West, Dezhou, 253023, China.
*E-mail addresses:* zhoumeng@iga.ac.cn (M. Zhou), jfyu1979@dzu.edu.cn (J. Yu).

temporal variations of $CH_4$ emissions from ruminants (Chang et al., 2019; Pérez-Barbería, 2017). Given that the recent Intergovernmental Panel on Climate Change (IPCC) report on the 'Impacts of 1.5 °C of Global Warming on Natural and Human Systems' provides evidence for the urgency of our short-term future plans (IPCC, 2022), only a tiny amount of atmospheric carbon credits remain before we reach the irreversible tipping point.

Recently, a Bayesian modeling analysis discovered that rumen microbiota influence dairy cattle $CH_4$ emission (Zhang et al., 2020). Specific enrichment of microbes and metabolic pathways was proposed to improve energy and carbon channeling, acccompanied by a decrease in $CH_4$ emission into the atmosphere (Kruger Ben Shabat et al., 2016). It is widely accepted that the production of $CH_4$ mainly comes from the function and metabolism of archaea. However, Metagenome and metatranscriptome analyses of the rumen in low $CH_4$-yielding sheep revealed lactic acid formation and utilization controlled by bacteria (Kamke et al., 2016), despite host-archaeal community interactions suggesting substantial $CH_4$ production (Borrel et al., 2020). Anaerobic fungi can also outcompete bacteria and archaea, playing a significant role in $CH_4$ release during polysaccharide degradation (Peng, 2021). These results provoke key fundamental questions: what are the drivers of the large $CH_4$ emissions from livestock waste, and are they related to microbial syntrophy processes, including changes in microbial community composition, diversity, activity, and developmental stages of host?

In this study, we analyzed whether and how methanogenic archaea form stable association with bacteria in diverse dairy cattle wastes from different developmental stages. Based on experimental results from kinetic analysis, stable isotope analysis, and metagenome-assembled genomes (MAGs), we hypothesized that a microbiota-first strategy, rather than a single-flora approach, restricts methanogenic strategies and their greenhouse effects.

## 2. Material and methods

### 2.1. Sample collection and cultivation experiments

Dairy cattle feces samples from different developmental stages were acquired at the Hebei Adopt A Dairy cattle™ Dairy Co. Ltd. The facility was environmentally controlled and maintained high hygiene standards. All dairy cattle were fed a similar standard corn–soy diet with a minimum metabolizable energy of ~3200 kcal/kg. The diet of 1 year(yr) old

[illegible]

rectal feces were collected from each group with at least 3 replicates.

For the cultivation experiments, 1 g fresh feces and 5 g of water were added to serum bottles. Vacuum/charging high-purity nitrogen (3 cycles) were conducted to establish an anaerobic environment. The bottles were kept at 30 °C in the dark for 22 days. Serum bottles were sacrificed in triplicate to test $CH_4$ and $CO_2$ concentrations. Tests for pH and acetate concentration was also performed. Stable isotope analysis was conducted on samples collected on day 22.

### 2.2. Chemical analysis

A gas chromatography (GC; Agilent 7820A, USA) equipped with a flame ionization detector (FID) was used to analyse biogas concentrations. Acetate concentration was measured using a high-performance liquid chromatography (HPLC) apparatus (Agilent 1260 Infinity) equipped with a refractive index detector (RID) referring to previous studies (Xiao et al., 2019).

### 2.3. Carbon stable isotope analysis

Carbon stable isotopes was measured using a gas chromatograph combustion isotope ratio mass spectrometer (GC–C–IRMS) system (Thermo Fisher MAT253, Germany). $CH_4$ and $CO_2$ were firstly separated by a Finnigan Precon. The separated $CH_4$ was injected into a 100 ml container prefilled with helium gas. The mixture was loaded into a chemical trap which can remove $CO_2$ and $H_2O$. Then, $CH_4$ can be oxidized to $CO_2$ and $H_2O$ in a combustion reactor at 960 °C. The obtained $CO_2$ was purified by two consecutive liquid nitrogen cold traps filled with Ni wires and analyzed by IRMS with a precision of ±0.2‰ for 1.3 nmol $CH_4$. The δ notation was used to denote the abundance of $^{13}C$ as follows (Xiao et al., 2019; Gehring et al., 2015):

$$\delta^{13}C = \left[ \frac{\left(\frac{^{13}C}{^{12}C}\right)_{sample}}{\left(\frac{^{13}C}{^{12}C}\right)_{PDB}} - 1 \right] \times 1000$$

where the standard is from Pee Dee Belemnite (PDB) carbonate with a $^{13}C/^{12}C$ ratio of 0.0112372. The measurement of $\delta^{13}C$-values of $CO_2$ was similar, where a water trap was used to replace the chemical trap. The α value can be calculated using the following equation (Xiao et al., 2019; Gehring et al., 2015):

$$\alpha = \frac{\delta^{13}CO_2 + 1000}{\delta^{13}CH_4 + 1000}$$

### 2.4. Calculation of Gibbs free energy for acetoclastic methanogenesis

For the calculation of ΔG of acetoclastic methanogenesis, the following equation is used:

$$\Delta G = \Delta G^0 + RT^* \left\{ \ln \left[ \frac{C_{CH_4} {}^* C_{CO_2}}{(C_{acetate})} \right] \right\} + 2.303 * RT * N_{pH}$$

where $\Delta G^0$, ΔG are the Gibbs free energy at 273.15 K and 101.325 kPa; Ris the ideal gas constant, 8.3145 J $mol^{-1}{\cdot}K^{-1}$; T is the absolute thermodynamic temperature, 303.15 K; $C_{CH_4}, C_{CO_2}$ and $C_{H_2}$ represent the concentrations of $CH_4$, $CO_2$, and $H_2$ in $mol{\cdot}L^{-1}$. For the calculation of $\Delta G^0$, use $\Delta G^0 = \Delta G_f^0 - \Delta S^*(T_f - T_0)$, where $\Delta G_f^0$ is the Gibbs free energy under 298.15 K and 101.325 kPa; ΔS is the entropy change at 298.15 K; $T_f$ and $T_0$ are 298.15 K and 273.15 K, respectively. $\Delta G_f^0$ is calculated as $\Delta G_f^0 = \Delta H - T_f{}^* \Delta S$, where ΔHis the enthalpy change at 298.15 K. $C_{acetate}$ is the acetate concentration in $mol{\cdot}L^{-1}$ and $N_{pH}$ is the pH value of the supernatant.

### 2.5. DNA extraction, separation, and sequencing

The samples at day 22 were collected for metagenomic sequencing. To verify the generalizability of the data, we collected dairy cattle samples from another city, Beijing Sanyuan Food Co. Ltd. (ShouGuang, China), for microbiome analysis. The E.Z.N.A.® Soil DNA Kit made by Omega Bio-tek, Norcross, GA, U.S. was used to extract the total DNA. The NEXTflex™ Rapid DNA-Seq Kit (Bio Scientific, Austin, TX, USA) was used to construct paired-end libraries. Adapters containing the full complement of sequencing primer hybridization sites were ligated to the blunt end of the fragments. The libraries were sequenced using Illumina Hiseq Xten technology (Illumina Inc., San Diego, CA, USA) at OEBiotech Co., Ltd. (Qingdao, China) using HiSeq X Reagent Kits according to the instructions from the manufacturer for 150 bp paired-end sequences. Sequence data associated with this project was deposited in the National Microbiology Data Center (Beijing, China) with under accession number NMDC10018086.

### 2.6. Assembly of metagenomic data sets

A Linux server equipped with 88 CPU cores and 1T RAM was used to conduct the *de novo* assembly of the metagenomic sequences. Trimmomatic was used to remove adapters and filter low quality reads (Bolger

et al., 2014). Contaminations were removed by aligning our reads to the human genome Hg38 using BBmap. The final clean reads from all eight samples were co-assembled using MEGAHIT with default parameters (Li et al., 2015). Finally, only contigs larger than 500 bp were selected for downstream analysis. QUAST was used to assess the quality of the assembly (Gurevich et al., 2013).

### 2.7. Genomic binning and annotation

The binning process was performed with MetaWRAP (Uritskiy et al., 2018). Briefly, the assembly was binned with MaxBin2 (Wu et al., 2016), MetaBAT2 (Kang et al., 2019), and CONCOCT (Alneberg et al., 2014) with the binning module, respectively. The produced MAGs were refined using the bin_refinment module with completeness >50%, contamination <10% as thresholds. The filtered MAGs were further improved using the bin_reassembly module, which reassemble the MAGs with SPAdes (Bankevich et al., 2012). The bin_quant module was used to quantify the final MAGs (Patro et al., 2017), and calculate the average counts for each MAG. Then each MAG was normalized as copies per million reads.

Taxonomy annotation of the MAGs was carried out using the Genome Taxonomy Database Toolkit (GTDB-Tk, Chaumeil et al., 2020). It first predicted the ORFs of the MAGs using Prodigal (Hyatt et al., 2010), then 120 single copy genes for bacteria and 122 single copy genes for archaea were retrieved and aligned using the GTDB database. The concatenated alignment was then used to build a phylogenetic tree. Meanwhile the average nucleotide identity (ANI) of the MAGs was calculated using FastANI (Jain et al., 2018). The taxonomy annotation was performed based on their position in the phylogenetic tree and the ANI similarity.

The ORFs in the MAGs were predicted using Prodigal (Hyatt et al., 2010) with default parameters. EggNOG-Mapper was used to annotate the final protein sequence files (Huerta-Cepas et al., 2017), aligning the protein sequences to the pre-built database and annotating their function, KEGG assignment, GO assignment, and COG assignment by the best hit. Carbohydrate-active enzymes (CAZys) were identified using dbCAN2 with the CAZy database (Zhang et al., 2018). The R package Vegan was used to perform PCoA analysis of Bray-Curtis distance based on KEGG and CAZy abundances.

The encoding of whole carbon metabolism pathways was inferred from genomes using KEGG modules, including both those available from KEGG and several custom modules (Table S1, Woodcroft et al., 2018). Pathway abundance was calculated as the average abundance of the individual steps within each pathway.

### 2.8. Phylogenetic analysis

The genomes were subjected to GTDB-Tk (Chaumeil et al., 2020) to align the single copy genes as described above. Then the concatenated alignments were used to build the phylogenetic tree using IQtree with 100 times bootstrap (Nguyen et al., 2014).

### 2.9. Composition analysis

We assessed the microbial composition at reads level using Kraken2 (Wood et al., 2019). With Kraken2, the reads were aligned with the RefSeq database, and the taxonomy assignments were selected through the LZW ancestor algorithm. The alpha diversity was calculated at species levels with the Microbiome package in R (www.r-project.org). Vegan was used to perform PCoA analysis of Bray-Curtis distance based on species count.

### 2.10. Bi-partite Co-occurrence network analysis

CoNet was used to construct the co-occurrence network of MAGs (with average abundance >1 copy per million reads and presented in at least two-thirds of the samples) using an ensemble approach combined with the ReBoot technique. Downstream analysis only considered the edges with FDR <0.05. Edge classified as "mutual exclusion" and "co-presence" represented negative (e.g., competitive) and positive (e.g., cooperative) relationship between pairs of MAGs, respectively. The bacteria-methanogen bi-partite network was generated by selecting connections between bacterial MAGs and methanogen MAGs.

### 2.11. Correlation analysis

The Pearson's correlation coefficient was calculated by the corAndPvalue function using the R package WGCNA (Langfelder and Horvath, 2008). The corresponding p values were adjusted by the Benjamini & Hochberg method through the R package multtest. The adjusted p value $< 0.05$ was considered statistically significant.

### 2.12. Statistical analysis

The comparison of the abundance of MAGs in different groups was calculated using R package limma. Only MAGs with adjusted $p < 0.05$ and $\log_2$ (fold change) $> 1$ or $< -1$ for all three comparisons were considered as significantly different MAGs.

## 3. Results

### 3.1. $CH_4$ production potential and pathways

Dairy cattle wastes used in this study (from four developmental stages: 1-, 1.5-, 2.5- and 4-year(yr)-old) showed distinct $CH_4$-producing potential (Fig. 1a). At the developmental stage (approximately 1-yr-old), it outcompeted other groups with a maximum $CH_4$ potential of 30 mM. The intermediate stage (2.5-yr-old) showed a significant decrease to 8 mM compared to the developmental stage ($p = 0.023$). The oldest group (4-yr-old) showed the lowest $CH_4$ potential (~5 mM) (Fig. 1a). Acetate concentration increased to 20 mM and then reduced to less than 3 mM for 1-yr-old group (Fig. 1b), demonstrating a positive production-consumption relationship with $CH_4$. Stable isotope analysis demonstrated that $\delta^{13}C$-$CH_4$ (Fig. S2) and the α-value (Fig. 1c) at the early stage were −40‰ and 1.025, respectively, falling within the range of typical acetoclastic methanogenesis. On the other hand, the oldest group showed a large proportion of $CO_2$ reduction to generate $CH_4$ with values of −60‰ and 1.05 for $\delta^{13}C$-$CH_4$ and the α-value, respectively. Feces from middle developmental stages appeared to produce $CH_4$ via both pathways (−50‰ and 1.04 for the 1.5-yr-old group, −45‰ and 1.03 for the 2.5-yr-old group, Fig. 1c). The Gibbs free energy of acetoclastic methanogenesis for the feces of 1-yr-old group increased slightly over the last days of the experiment, but remained below −20 kJ $mol^{-1}$ (Fig. 1d). The Gibbs free energy for the other groups was under −40 kJ $mol^{-1}$ and varied scarcely during the cultivation period.

### 3.2. Recovery and distribution of MAGs

We obtained over 120 Gbp of high-quality metagenome sequencing data. The high-quality reads obtained were also co-assembled, resulting in 304,847 contigs with an N50 of 8288 bp. A total of 288 unique bacterial (279 MAGs) and archaeal (9 MAGs) genomes were recovered through genome binning after co-assembly (Table S2), including 67 high-quality MAGs (completeness >95% and contamination <5%) and 221 medium quality MAGs (completeness >50% and contamination <10%). The overall average completeness and contamination were 82.38% and 3.71%, respectively. The recovered MAGs spanned 13 phyla, including bacteria from Firmicutes (104 MAGs), Bacteroidetes (81 MAGs), and Proteobacteria (58 MAGs), and archaea from the phylum Euryarchaeota (9 MAGs) (Fig. S3). Consistent with the heterogeneity of feces in the environment, individual MAGs with high abundance (over 1%) were found in a limited number of samples. For several

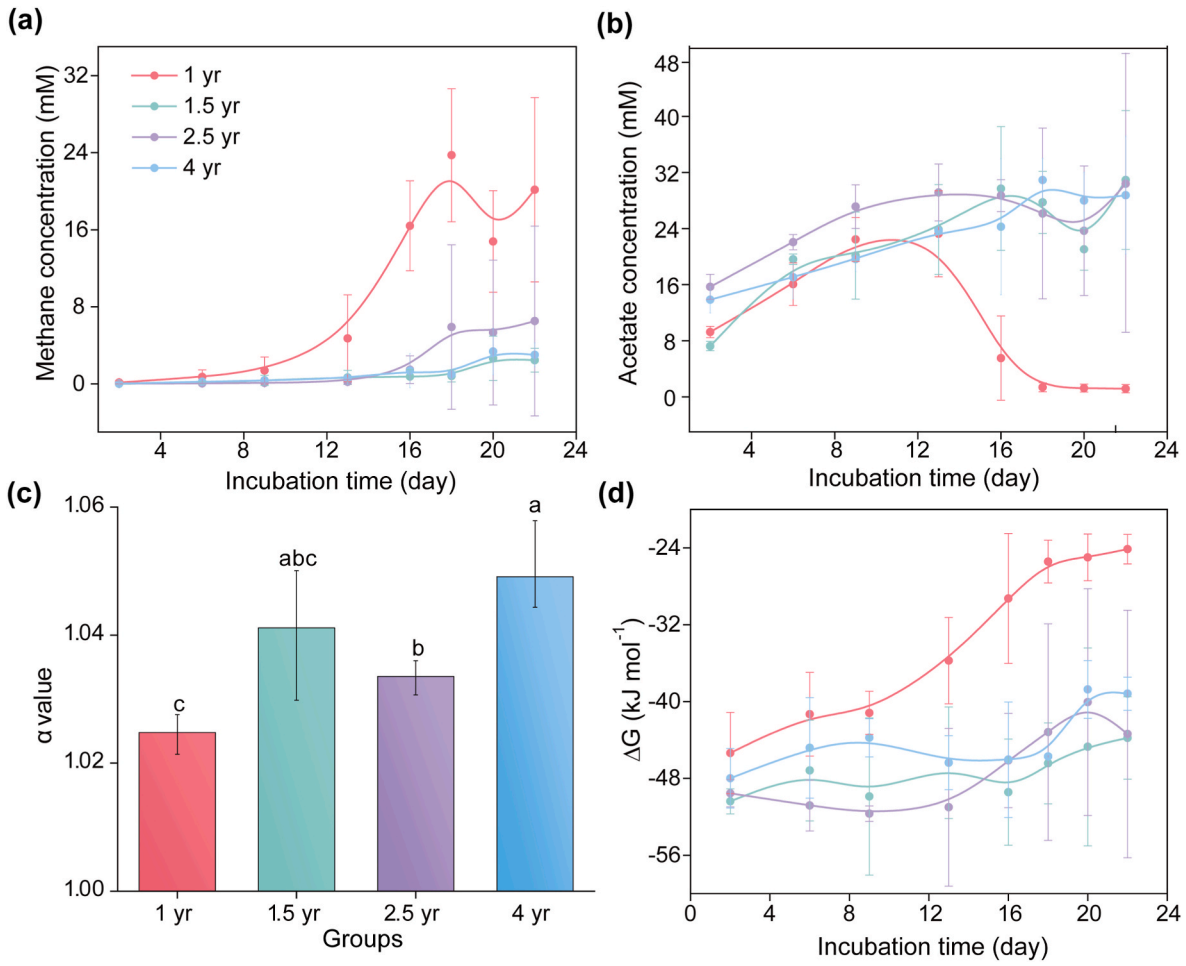


**Fig. 1.** $CH_4$ production strategies of dairy cattle feces. (a) $CH_4$ concentration; (b) acetate concentration; (c) α-value; (d) Gibbs free energy of acetoclastic methanogenesis dynamics.

genera, closely related MAGs were abundant in the feces from the four developmental stages (Table S2), reflecting a fine-scale adaptation to distinct niches in the rumen and gut.

The microbiome diversities were analyzed at the reads level, revealing no significant differences in alpha diversity indices, including Chao1, Shannon, and Inverse Simpson Index (Fig. 2a, one-way analysis of variance (ANOVA), $p > 0.05$). Microbial community structures were strongly correlated with habitat changes, as demonstrated by abundance mapping across developmental gradients (Fig. 2b, permutational multivariate analysis of variance (PERMANOVA), $p = 0.023$). At the phylum level, Proteobacteria consistently dominated (>50%), followed by Bacteroidetes (~20%) and Firmicutes (~8%) (Fig. 2c). Notably, the proportion of Euryarchaeota decreased from 3% in the 1-year-old group to just 1% in the 4-year-old group, dropping to the seventh most abundant component.

### 3.3. *Polysaccharide degradation*

The potential microbes, pathways, and interactions responsible for the degradation of polymeric organic matter and $CH_4$ production were evaluated by examining the metabolic reconstruction of the acquired MAGs (Fig. 3; Table S3). The breakdown of high molecular-weight plant-derived polysaccharides was involved in the first stage, primarily cellulose and hemicellulose. Cellulase- and xylanase-encoding microorganisms primarily belonged to the phylum Bacteroidetes (Fig. 3, MAG abundances). For cellulase-encoding microorganisms, Bacteroidetes was the most abundant phylum in the feces from all four stages (31.0%, 25.9%, 36.2% and 30.4% of the recovered community in the 1-, 1,5-, 2,5- and 4-yr-old group, respectively), with a slight decrease in 1.5 yr-old stage. For xylanase-encoding microorganisms, the abundance of Bacteroidetes was similar across all four stages (24.4%, 24.9%, 24.0% and 29.0% of the recovered community in the 1-, 1,5-, 2,5- and 4-yr-old group, respectively). The xylan-degrading microorganisms showed a high similarity to cellulose degraders, whereas in the feces of 2.5- and 4-yr-old groups, this metabolism was limited to a high number of Bacteroidetes and a smaller number of Firmicutes (Fig. 3). Cellulase-encoding Bacteroidetes with high relative abundances (77.1%, 56.4%, 86.8% and 77.0% of the recovered community in the 1-, 1,5-, 2,5- and 4-yr-old group, respectively) and xylanase-encoding Bacteroidetes (70.2%, 57.7%, 88.5% and 82.9% of the recovered community in the 1-, 1,5-, 2,5- and 4-yr-old group, respectively), strongly suggested that the primary degraders of large polysaccharides belonged to this phylum in dairy cattle feces, but polysaccharide degradation seemed not to be the key factor in controlling $CH_4$ production.

Microbial communities seek primary sources of energy and carbon by breaking down polysaccharides into simple sugars. β-Glucosidases for disaccharide degradation were encoded by microorganisms, predominantly within the Bacteroidetes phylum across all microbiomes (Fig. 3). Firmicutes were also detectable in all the samples with lower abundance, as were Fibrobacteres and Spirochaetes. Bacteroidetes was the dominant phylum, which occupies every stage of development: 1 yr-old group (81.0% of the microbial community), 1.5-yr-old group (57.5%), 2.5-yr-old group (91.4%) and 4-yr-old group (90.4%).

MAGs were also abundant in the degradation of monosaccharides

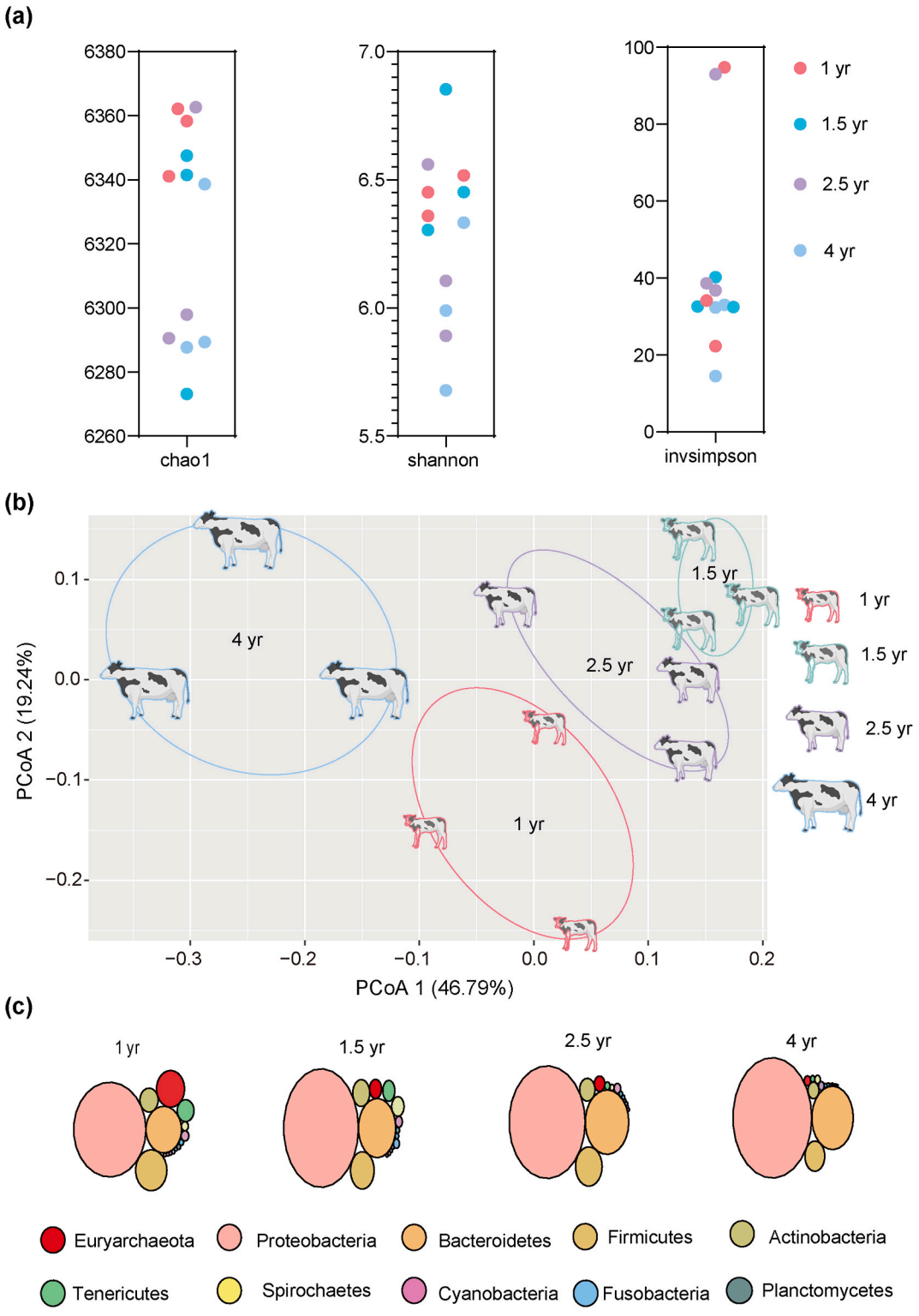


**Fig. 2.** The reads composition of the fecal microbiome for distinct dairy cattle. (a) α diversities at reads level of the gut microbiome; (b) PCoA analysis based on the Bray-Curtis distance of the samples; (c) The composition at the phylum level of the gut microbiome. Note: The size of the dairy cattle diagram in (b) only represents the difference in developmental stages, not their body size.

such as glucose, galactose, lactose and xylose (Table S3). Fructose did not appear to be an important intermediate metabolite during polysaccharide degradation. Glucose, galactose and lactose were degraded by the same community composition (Fig. 3), but the microbial community composition varied considerably among the feces from different developmental stages of daily cattle. Glucose-degrading microorganisms showed very high similarity to those that degrade galactose. Bacteroidetes acted as the key player in monosaccharide degradation. The importance of Proteobacteria gradually manifested across developmental stages. In this case, Bacteroidetes and Proteobacteria shared a fifty-fifty basis of abundance. Interestingly, MAGs belonging to Euryarchaeota also encoded pathways for glucose and galactose utilization,

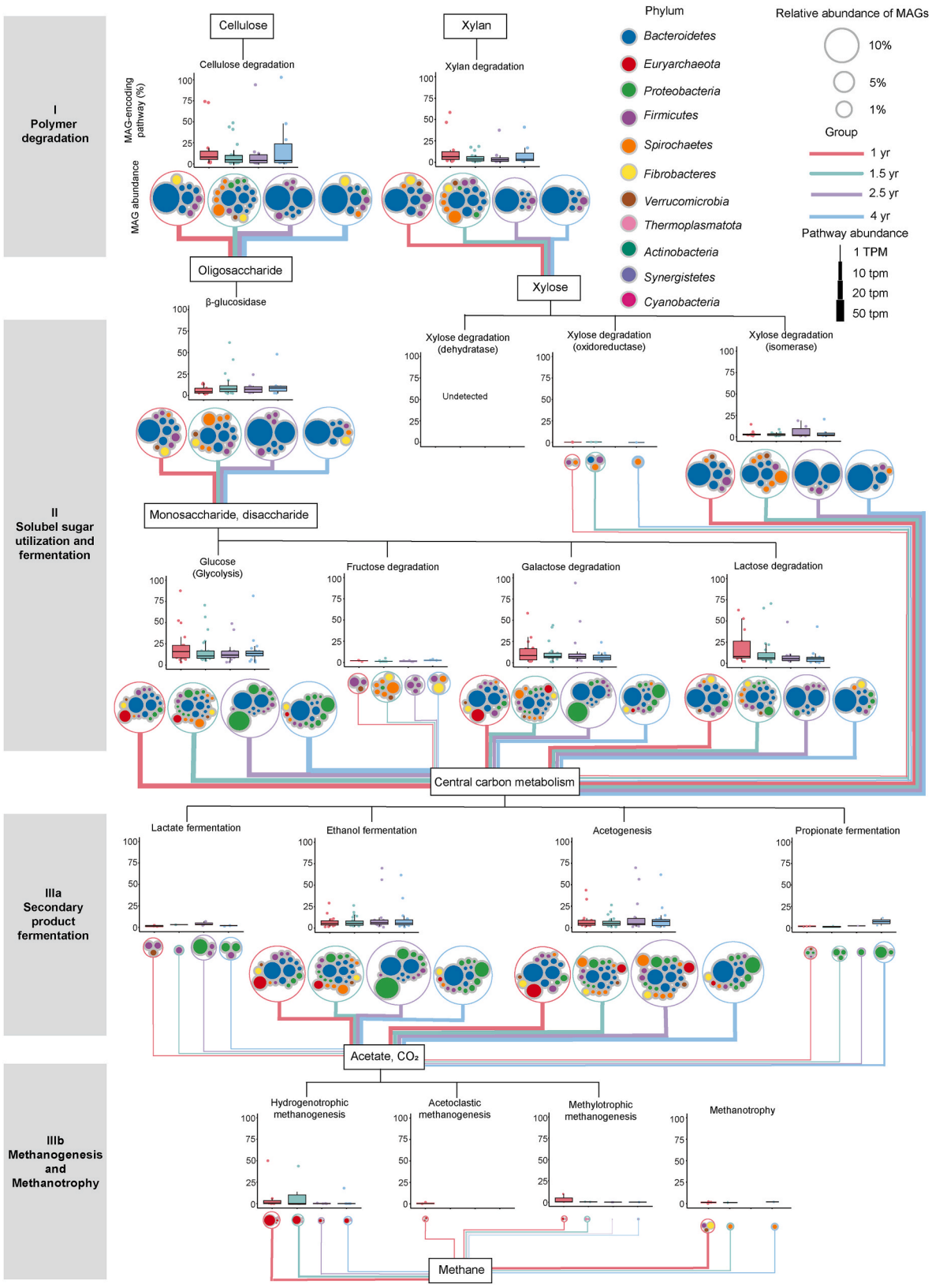


**Fig. 3.** Microbial carbon metabolism in feces from dairy cattle at different developmental stages. The Grey boxes in the left indicate the fermentation processes. White box plot headers and carbon compound boxes show degradation pathways. The large circles have outlines colored by group, and contain smaller circles (MAG abundances, colored by phylum) representing the different MAGs containing genes encoding for pathways described in the scheme. Circle size indicates MAG average relative abundance. The distribution box plots are colored by group. Box plot y axes indicate the cumulative relative abundances of the MAGs containing genes encoding pathway of interest in each group, which also showed by the line thickness connecting the intermediates.

comprising 13.5% and 7.3% of the community in the early developmental stages, respectively. At later stages, glucose and galactose degradation was identified in Proteobacteria MAGs. For lactose degradation, the contribution of Bacteroidetes ran through the whole developmental stages by different Bacteroidetes classes.

The degradation pathways for monosaccharides through fermentation and acetogenesis are essential for supplying substrates for methanogenesis. Low-molecular-weight alcohols and organic acids such as ethanol, propionate, acetate, and lactate, as well as hydrogen and $CO_2$ can be produced during the fermentation stage. In dairy cattle feces, the microorganisms involved in ethanol metabolism overlapped almost perfectly with those involved in glucose degradation. In brief, ethanol fermentation is encoded by MAGs from the phyla Bacteroidetes and Proteobacteria (Fig. 3), which were particularly abundant in feces from older dairy cattle (72.6% and 56.8% of the community for 2.5- and 4-yr, respectively). Populations of Proteobacteria appeared to be an important propionate metabolizer (3.6%, 4.0%, 2.4% and 14.4% for 1-, 1,5-, 2,5- and 4-yr-old group, respectively). Yet, their low abundance weakened the contribution of propionate metabolism to overall $CH_4$ production, which also held true for lactate metabolism. Functional microorganisms involved in acidogenic metabolism were similar to those involved in glycolysis and ethanol fermentation, with a predominance of Bacteroidetes. Interestingly, a fraction of Euryarchaeota and Proteobacteria genomes were capable of acetogenesis (Fig. 3), and a contribution of this pathways was mainly limited to Euryarchaeota for the feces of the younger groups and Proteobacteria for the older group.

For methanogenesis, hydrogenotrophic methanogens basically increased in abundance from 1- to 4-yr-old groups (Fig. 3), which was not consistent with the increase in $CH_4$ accumulation. Unexpectedly, Thermoplasmatota were found in all samples, suggesting there potential role in $CH_4$ production. Only two low-abundant acetoclastic methanogens were recovered exclusively from feces of 1-yr-old group, MAG.271 and MAG.209 (Fig. S5). Methylotrophic methanogens from Euryarchaeota and Thermoplasmatota were also recovered, but Euryarchaeota were present only in the 1-yr-old group at a low abundance (0.6%). Methanotrophs from Firmicutes, Fibrobacteres, Verrucomicrobia and Spirochaetes were also identified. Their high abundances in the feces of the 1-yr-old group suggested methanotrophs may oxidize some proportions of $CH_4$.

### 3.4. Bacteria-methanogen bi-partite co-occurrence network

We also identified 57108 genes with carbohydrate-active enzyme (CAZy) activity, belonging to 259 CAZy families (Fig. S5). Key functional microorganisms and genes were analyzed and discussed (Figs. S5–S7, Tables S4 and S5). Bi-partite co-occurrence network analysis of bacteria-methanogen associations showed that bacteria nodes occupied a dominant proportion suggesting the importance of bacteria in the microbiomes for $CH_4$ production (Fig. 4a). Firmicutes and Bacteroidetes were the main contributors to this process (Fig. 4a). The four bacteria-methanogen networks with host development contained 4, 3, 2, and 1 archaeal MAGs, respectively (Fig. 4b). The number of the edges in these networks was 104, 95, 75, and 41, while the number of nodes was 68, 87, 43 and 38. Both edges and nodes gradually decreased. About 57.7% of the edges (60 out of 104) in the first group showed co-occurrence interactions. Also, about 64.2% (59 out of 95), 72% (54 out of 75), and 70.7% (29 out of 41) showed co-occurrence interactions in the other groups (Fig. 4b). Thus, the feces from daily cattle at the early stage had the strongest selectivity of bacteria-archaea association among the four stages.

Archaea node percentages gradually decreased with age, suggesting a weaker co-occurrence of methanogenic archaea in later stages (Fig. 3a). MAG.271, belonging to *Methanosarcinaceae*, although at lower abundance than MAGs belonging to *Methanocorpusculaceae,* showed more connections with bacterial MAGs (34 vs 18, Fig. 3b), further confirming the crucial contribution of this low abundant methanogen. The network for feces from the 4-yr-old group contained only a hydrogenotrophic methanogen, MAG.189 (Fig. 4b), which was in accordance with the isotope analysis results showing that this group produced $CH_4$ mainly through $CO_2$ reduction.

### 3.5. $CH_4$ production affected by functional activity

Over 200 million genes were identified in the metagenomic data, belonging to 5846 KEGG gene orthologs. No noticeable differences were found among the four groups according to alpha diversities of KEGG gene orthologs (Shannon and Inverse Simpson Index, Figs. S8a and b). Nearly all genes involved in methanogenesis were positively correlated with $CH_4$ production (Fig. 5a). The correlation, however, was not statistically significant ($p = 0.216$), suggesting that methanogenic progress was potentially influenced by other factors. The PCoA analysis on the Bray-Curtis distance calculated by KEGG gene ortholog abundances showed distinct structures (Fig. S8c). Therefore, the differences in the metabolism of microbiomes existed in the feces from diverse developmental stages.

By analysing all the groups together, no significant associations were observed between the compositional parameters of KEGG orthologs and $CH_4$ production parameters (Fig. b, *p*-values in Table S6). This may be related to the large fluctuations in microbial diversity, abundance, and function (Fig. b). The first axis (PCoA1) of CAZy families, however, was positively correlated with $\delta^{13}C\text{-}CH_4$, but negatively correlated with α-value, indicating the importance of CAZy families for methanogenic pathways. We further analyzed the key controlling factors of $CH_4$ production. For the early stage, bacterial PCoA1 was positively correlated with acetate production and consumption. CAZy synthesis, which are performed by bacteria, significantly affected $CH_4$ accumulation ($p = 0.033$), further confirmed that bacteria constrained $CH_4$ production.

## 4. Discussion

Worldwide $CH_4$ emissions from agricultural livestock continuously increase during the last few decades (Fig. S1b) and will expect linear growth in the future (Eshel et al., 2014). It is predicted that $CH_4$ generated from livestock microbiomes will reach 110 and 122 Tg by 2030 and 2050, respectively (Fig. S1b). Anthropogenic emissions (356 Tg/a) account for about two-thirds of total emissions, of which livestock accounts for 100–117 Tg/a, emanating either from the biowaste generated by farms, such as feces and/or manure, or directly by exhalation (Maasakkers et al., 2019). As shown in Fig. S1c, high dairy cattle stocking (265 million in 2019) and ruminant behavior results in $CH_4$ releases accounting for about one-quarter of the total livestock. Feces and manure microbiomes are receiving increasing attention in managing $CH_4$ emissions (Difford et al., 2018; Wallace et al., 2019).

In general, the abundance of methanogens is correlated to high methane emissions, whereas no other direct correlations have been reported (Kruger Ben Shabat et al., 2016; Zhou et al., 2009). These inconsistencies lie in the lack of clarity on the key microbiomes for $CH_4$ production. As reported, the genus *Methanobrevibacter* (*Methanobacteriales* order) is dominant, accounting for up to 70% of the rumen archaeal community (Borrel et al., 2020; Friedman et al., 2017). However, *Methanobrevibacter* seemed not to be a crucial methanogenic archaeon in this study, especially in the feces from the early developmental stage, where they were found to be only 0.017% abundance (Fig. S5). Our results also revealed that archaea with the ability to produce $CH_4$ were also found in the phylum Thermoplasmatota, suggesting diverse linkages of methanogenic archaea (Fig. 3, Table S3). Methanogen is not the only factor determining $CH_4$ production potential (Figs. 1 and 3), and the relationship between $CH_4$ production and microbiome structure remains largely uncertain. However, the variation in composition of the core bacteria and archaea was successfully used to predict the amounts of $CH_4$ emissions with high accuracy (Evans et al., 2015) (Fig. S9, Table S7). Low-abundance taxa, such as *Methanosarcina*, showed close

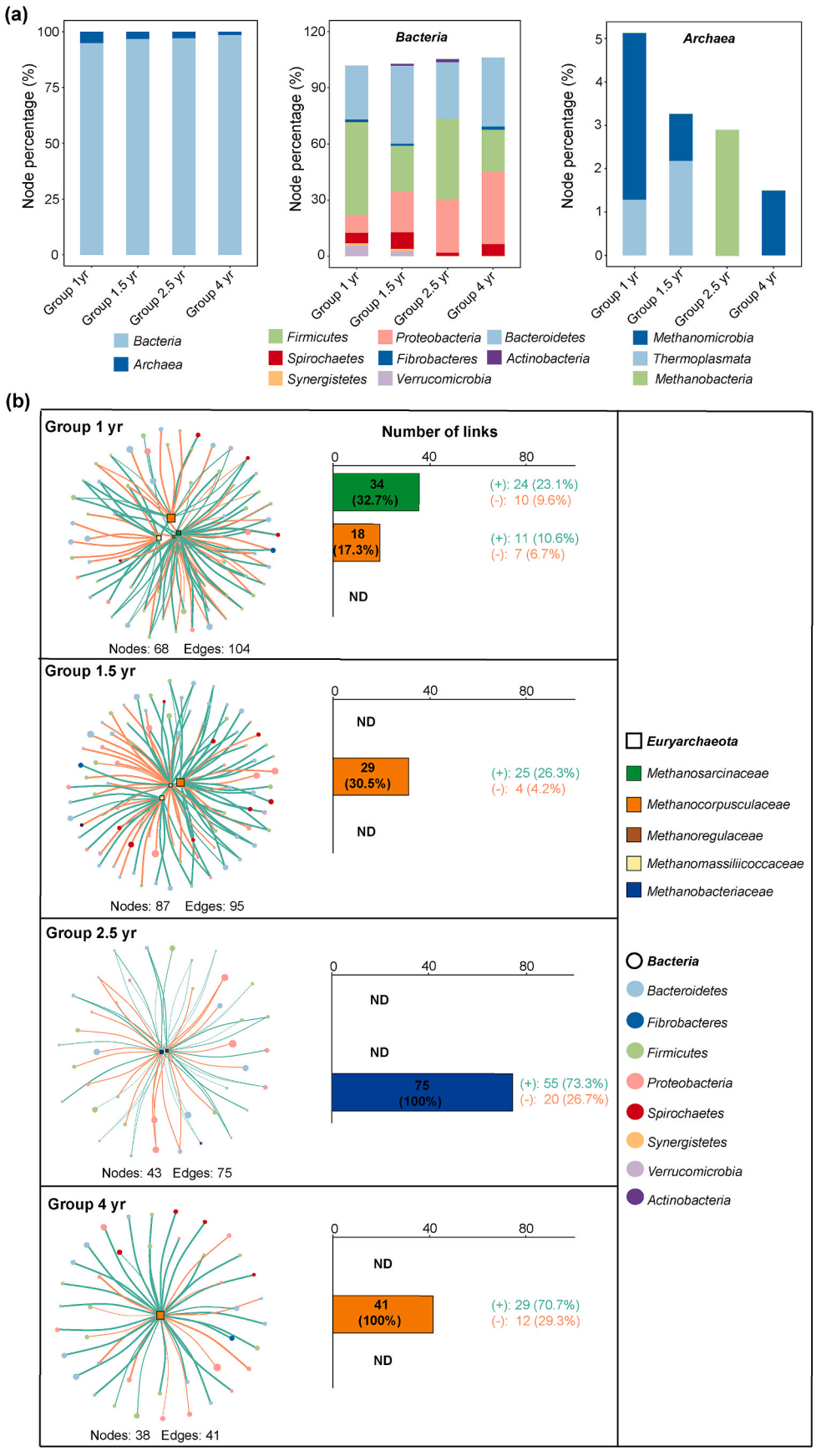


*(caption on next page)*

**Fig. 4.** Bacteria-methanogen bi-partite co-occurrence networks. (a) Node percentage of different taxonomy levels within the networks. (b) Links between bacterial MAGs and methanogen MAGs. Bar plot showed the number of links between bacterial MAGs and methanogen MAGs of *Methanosarcinaceae*, *Methanocorpusculaceae*, and *Methanobacteriaceae*. Green lines denoted co-occurrence (+). Orange lines denoted exclusion (−). Line width denoted the weight of the associations. (For interpretation of the references to colour in this figure legend, the reader is referred to the Web version of this article.)

associations with predominant members (Fig. 4, S5). The microbial web of interactions in the microbiome defined the ultimate community composition, function and, thus, outcome ($CH_4$ production) (Figs. 1, 4 and 5). In the different developmental stages studied in the present study, the rumen ecosystem was stabilized at several alternative microbiome states depending on the microbial interaction types and the strength of the resulting metabolic feedback (Fig. 3 and), agreed with previous study (Vanwonterghem et al., 2016). Despite the initial species pool showing a long-lasting effect on the assembly process and adult composition of the feces microbiome (Poulsen et al., 2013), there were substantial differences in the functional microbial abundance with temporal change (Fig. S5).

We categorized microorganisms using similar input and output metabolites into functional groups guiding assemblies. All metabolic cascades of the feces from distinct developmental stages were carried out by the microbial community in a complex and coordinated manner, whereby successive cross-feeding across food webs existed among a diverse collection of microbes (Fig. 3). Kamke et al. (2016) found a high hydrogenotrophic methanogenic gene expression of sheep gastrointestinal tract. Similarly, the hydrogenotrophic methanogen, *Methanobrevibacter* was more active in ruminants with strong $CH_4$ production (Sasson et al., 2017). It was suggested that methanogenic archaea, and in particular *Methanobrevibacter* species, are extraordinarily well-adapted to interact with animal hosts and non-archaeal components of their microbiomes (Borrel et al., 2020). As our findings in the 2.5-yr-old group, *Methanobrevibacter* was indeed the most abundant, 14.6 times more abundant than the other groups combined. It is worth noting that a higher proportion of Euryarchaeota in the 1-yr-old group relative to the 2.5-year-old group was observed, implying that other Euryarchaeota taxa may be more prominent in the 1-yr-old group, contributing to the overall higher concentration of Euryarchaeota. Besides, the benefit from CAZys encoding for degradation of pectate and oligogalacturonate with an increased trend in the feces from later developmental stages, such as PL-10, GH138, and GH 139 (Fig. S4c), suggests the improvement of macromolecular carbon utilization efficiency. Due to the predominance of hydrogenotrophic methanogenesis by *Methanobrevibacter*, there was a high probability that the metabolic flow proceeds in the following order: polysaccharides, soluble sugar (glucose, galactose, lactose), $H_2$ and $CO_2$, $CH_4$.

Extreme high biogas accumulation, however, was found in the feces from the early developmental stage and speculated that metabolic cascades contribute to polysaccharide degradation. Carbohydrate-active enzymes preferred classical polysaccharides (Fig. S5c). Soluble sugar utilization to central carbon metabolism is a crucial pathway which can provide sufficient substrates, such as acetate, for subsequent metabolism (Moraïs and Mizrahi, 2019). The establishment of a robust stable community, mainly from Bacteroidetes and Euryarchaeota, is connected to $CH_4$ emission. The isotope evidence confirmed that $CH_4$ was reliably derived from the direct disproportionation cracking of acetate (Fig. 1, S2). Therefore, its unique acetoclastic methanogenesis pathway was also the guarantee of high $CH_4$ production (Furman et al., 2020; Greening et al., 2019). Isotope analysis also confirmed that acetoclastic methanogenesis was prevalent in diverse anaerobic systems (Greening et al., 2019; Han et al., 2017; Xiao et al., 2020a, 2020b; Li et al., 2018), which were previously believed to be dominated by $CO_2$ reduction pathway (Yu et al., 2022; Park et al.; Xiao et al., 2018). The prevalence of direct interspecies electron transfer (DIET) in the past decade may cover the inherent methanogenic strategy (Morita et al., 2011; Rotaru et al., 2014; Wegener et al., 2015). In this study, the analysis of electroactive microorganisms revealed that these bacteria were in very low abundance (Fig. 2, Fig. S6). The negative correlation of these microbial abundances with $CH_4$ production potential denied this possibility of $CH_4$ from electron reduction of $CO_2$.

Network analysis clearly supported a microbiota-first strategy, with targeted corporation driving enhanced $CH_4$ emission (Fig. 3). In there, the low abundance of *Methanosarcinaceae* outcompeted the high abundance of *Methanocorpusculaceae*, involving a large number of nodes and edges, and evenly distributed multiple interaction types (Fig. 3b). Stoichiometric results (acetate consumption and $CH_4$ production) also showed a perfect match via acetoclastic pathway rather than $CO_2$ reduction (Fig. 1), as our previous study evidenced (Xiao et al., 2020a). Thus, in the 1-year-old group, the acetoclastic methanogens (*Methanosarcinaceae*, MAG.271) and related bacteria formed a targeted cooperative network for methane production through acetate dissimilation. Similarly, in the 4-year-old group, Methanocorpusculaceae (MAG.189) formed a targeted cooperation for CO2 reduction. Combined microbiomes, rather than individual methanogens even with the highest abundance, controlled methane-producing potential. For Gibbs free energy of acetoclastic methanogenesis, this pathway was always thermodynamically feasible (Fig. 1d). The major metabolic flux for powerful $CH_4$ production in the feces from the early developmental stage holds polysaccharides, soluble sugar (glucose, galactose, lactose), acetate and $CH_4$. Nevertheless, open questions also include what the precise functions are in the highly abundant methanogens.

## 5. Conclusion

This study proved almost 6 times higher $CH_4$ production of young dairy cattle manure compared to older ones. Metagenomic assembled genomes analysis revealed the methane producing metabolic flux. Powerful $CH_4$ production potential was achieved via typical acetoclastic methanogenesis, which is validated through stable isotope and network analysis. However, a cooperative model dominated by hydrogenotrophic methanogenic archaea presented weak $CH_4$ production. Our findings comprehensively link carbon and $CH_4$ metabolism paradigms to specific microbial lineages, which are shaped by the developmental stages of dairy cattle. In conclusion, the interplay between microbial community composition, metabolic pathways, and microbial interactions plays a crucial role in the higher $CH_4$ production observed in young dairy cattle manure. Specifically, the dominance of acetoclastic methanogens, the higher proportion of Euryarchaeota taxa, the close interactions between bacteria and methanogens, and the presence of carbohydrate-active enzymes all contribute to the enhanced methane production in younger cattle manure. These factors emphasize the significant influence of microbial dynamics and metabolic processes on $CH_4$ output.

## Funding

This work was supported by the Natural Science Foundation of Heilongjiang Province in China (YQ2023D007), the Youth Innovation Promotion Association of CAS (2021213), the National Natural Science Foundation of China (42307437, 42077025, 42277236), the Youth Science and Technology Innovation Plan of Universities in Shandong (2019KJE007), and Research Project of Dezhou University (2023XKZX004). M.H. gratefully acknowledges Royal Society Dorothy Hodgkin Research Fellowship (DHF\R1\211076).

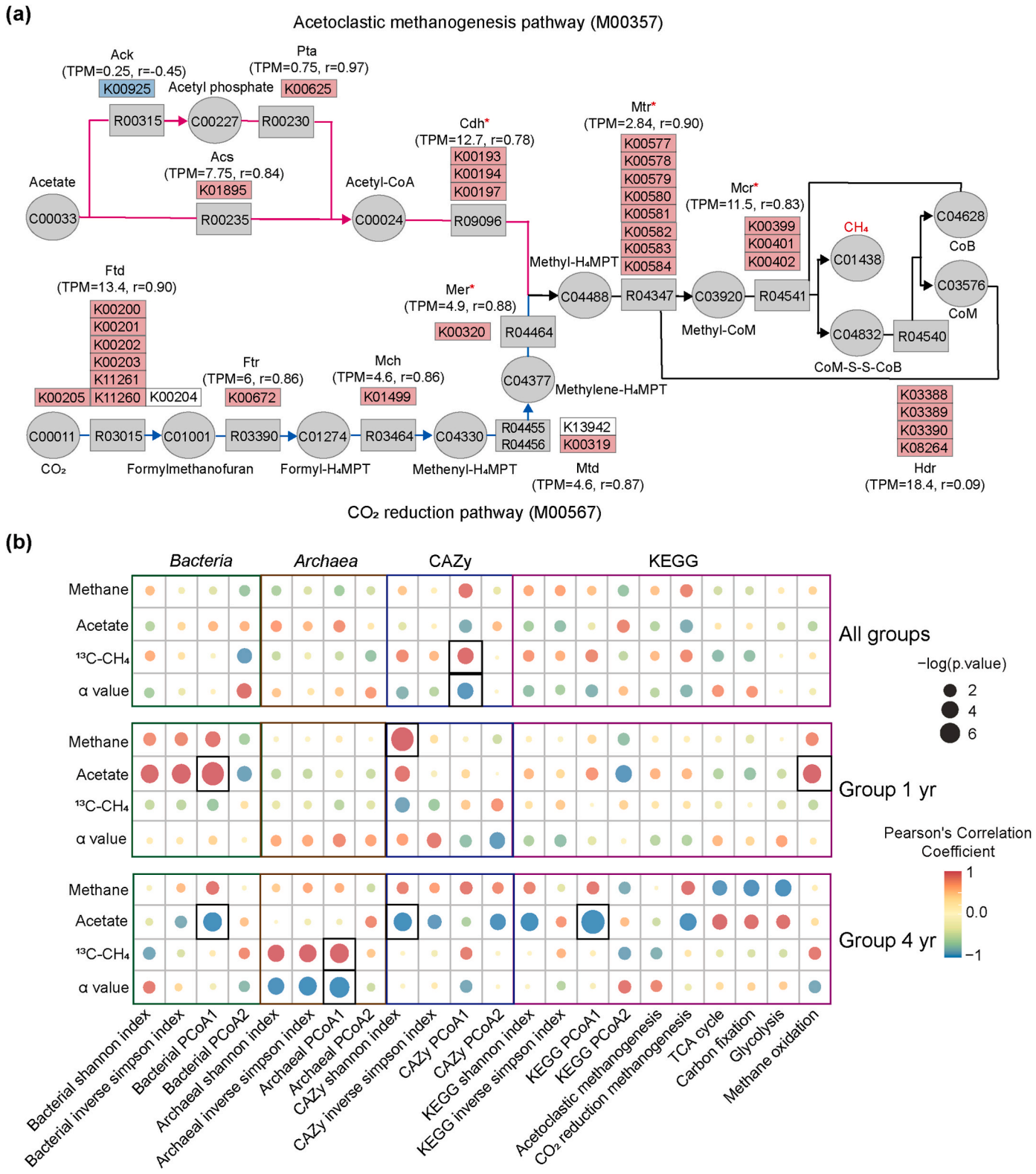


**Fig. 5.** Relationship between microbiome activities and $CH_4$ production. (a) Functional gene orthologs of methanogenesis in KEGG module M00567 and M00357. The red and blue colours indicated positive and negative correlations between KEGG gene orthologs and $CH_4$ production. White colours indicated undetected orthologs. Red asterisks indicated significant different orthologs ($p < 0.05$) between the 1-yr-old group and other groups. (b) Correlations between the methanogenesis parameters and the compositional parameters at different levels. The colour of the circles indicated Pearson's correlation coefficient. The size of the circles indicated negative log10 transformed p-value. The black boxes indicated $p < 0.05$. PCoA1 and PCoA2 indicated the first and second axes during PCoA analysis baseed on Bray-Curtis distance. (For interpretation of the references to colour in this figure legend, the reader is referred to the Web version of this article.)

## CRediT authorship contribution statement

**Jian Liu:** Writing – review & editing, Writing – original draft, Visualization, Methodology, Investigation. **Meng Zhou:** Writing – review & editing, Visualization, Investigation. **Lifeng Zhou:** Methodology. **Run Dang:** Investigation. **Leilei Xiao:** Writing – review & editing, Writing – original draft, Visualization, Methodology, Investigation, Conceptualization. **Yang Tan:** Methodology. **Meng Li:** Investigation. **Jiafeng Yu:** Writing – original draft, Visualization, Supervision, Methodology, Investigation. **Peng Zhang:** Visualization. **Marcela Hernández:** Writing – review & editing, Writing – original draft, Methodology. **Eric Lichtfouse:** Writing – review & editing, Writing – original draft, Investigation.

## Declaration of competing interest

The authors declare that they have no known competing financial interests or personal relationships that could have appeared to influence the work reported in this paper.

## Appendix A. Supplementary data

Supplementary data to this article can be found online at https://doi.org/10.1016/j.envres.2024.120642.

## Data availability

Data will be made available on request.

## References


Alneberg, J., Bjarnason, B.S., de Bruijn, I., Schirmer, M., Quick, J., Ijaz, U.Z., Lahti, L., Loman, N.J., Andersson, A.F., Quince, C., 2014. Binning metagenomic contigs by coverage and composition. Nat. Methods 11, 1144–1146. https://doi.org/10.1038/nmeth.3103.

Bankevich, A., Nurk, S., Antipov, D., Gurevich, A.A., Dvorkin, M., Kulikov, A.S., Lesin, V. M., Nikolenko, S.I., Pham, S.K., Prjibelski, A.D., Pyshkin, A., Sirotkin, A., Vyahhi, N., Tesler, G., Alekseyev, M.A., Pevzner, P.A., 2012. SPAdes: a new genome assembly algorithm and its applications to single-cell sequencing. J. Comput. Biol. 19, 455–477. https://doi.org/10.1089/cmb.2012.0021.

Bhattacharya, S.C., Thomas, J.M., Salam, P.A., 1997. Greenhouse gas emissions and the mitigation potential of using animal wastes in Asia. Energy 22, 1079–1085. https://doi.org/10.1016/S0360-5442(97)00039-X.

Boetius, A., 2019. Global change microbiology — big questions about small life for our future. Nat. Rev. Microbiol. 17, 331–332. https://doi.org/10.1038/s41579-019-0197-2.

Bolger, A.M., Lohse, M., Usadel, B., 2014. Trimmomatic: a flexible trimmer for Illumina sequence data. Bioinformatics 30, 2114–2120. https://doi.org/10.1093/bioinformatics/btu170.

Borrel, G., Brugère, J.F., Gribaldo, S., Schmitz, R.A., Moissl-Eichinger, C., 2020. The host-associated archaeome. Nat. Rev. Microbiol. 18, 622–636. https://doi.org/10.1038/s41579-020-0407-y.

Chang, J.f., Peng, S.S., Ciais, P., Saunois, M., Dangal, S.R.S., Herrero, M., Havlik, P., Tian, H.Q., Bousquet, P., 2019. Revisiting enteric methane emissions from domestic ruminants and their $\delta^{13}CCH_4$ source signature. Nat. Commun. 10. https://doi.org/10.1038/s41467-019-11066-3, 2441-1723 3420.

Chaumeil, P.A., Mussig, A.J., Hugenholtz, P., Parks, D.H., 2020. GTDB-Tk: a toolkit to classify genomes with the genome taxonomy database. Bioinformatics 36, 1925–1927. https://doi.org/10.1093/bioinformatics/btz848.

Dangal, S.R.S., Tian, H., Zhang, B., Pan, S.F., Lu, C.Q., Yang, J., 2017. Methane emission from global livestock sector during 1890-2014: magnitude, trends and spatiotemporal patterns. Glob. Chang Biol. 23, 4147–4161. https://doi.org/10.1111/gcb.13709.

Difford, G.F., Plichta, D.R., Løvendahl, P., Lassen, J., Noel, S.J., Højberg, O., Wright, A.G., Zhu, Z., Kristensen, L., Nielsen, H.B., Guldbrandtsen, B., Sahana, G., 2018. Host genetics and the rumen microbiome jointly associate with methane emissions in dairy cows. PLoS Genet. 14, e1007580. https://doi.org/10.1371/journal.pgen.1007580.

Eshel, G., Shepon, A., Makov, T., Milo, R., 2014. Land, irrigation water, greenhouse gas, and reactive nitrogen burdens of meat, eggs, and dairy production in the United States. Proc. Natl. Acad. Sci. U.S.A. 111, 11996–12001. https://doi.org/10.1073/pnas.1402183111.

Evans, P.N., Parks, D.H., Chadwick, G.L., Robbins, S.J., Orphan, V.J., Golding, S.D., Tyson, G.W., 2015. Methane metabolism in the archaeal phylum Bathyarchaeota revealed by genome-centric metagenomics. Science 350, 434–438. https://doi.org/10.1126/science.aac7745.

Friedman, N., Shriker, E., Gold, B.S., Durman, T., Zarecki, R., Ruppin, E., Mizrahi, I., 2017. Diet-induced changes of redox potential underlie compositional shifts in the rumen archaeal community. Environ. Microbiol. 19, 174–184. https://doi.org/10.1111/1462-2920.13551.

Furman, O., Shenhav, L., Sasson, G., Kokou, F., Honig, H., Jacoby, S., Hertz, T., Cordero, O.X., Halperin, E., Mizrahi, I., 2020. Stochasticity constrained by deterministic effects of diet and age drive rumen microbiome assembly dynamics. PLoS Comput. Biol. 13, e1005404. https://doi.org/10.1038/s41467-020-15652-8.

Gehring, T.A., Klang, J., Niedermayr, A., Berzio, S., Immenhauser, A., Klocke, M., Wichern, M., Lübken, M., 2015. Determination of methanogenic pathways through carbon isotope ($\delta^{13}C$) analysis for the two-stage anaerobic digestion of high-solids substrates. Environ. Sci. Technol. 49, 4705–4714. https://doi.org/10.1021/es505665z.

Greening, C., Geier, R.R., Wang, C., Woods, L.C., Morales, S.E., McDonald, M.J., Rushton-Green, R., Morgan, X.C., Koike, S., Leahy, S.C., Kelly, W.J., Cann, I., Attwood, G.T., Cook, G.M., Mackie, R.I., 2019. Diverse hydrogen production and consumption pathways influence methane production in ruminants. ISME J. 13, 2617–2632. https://doi.org/10.1038/s41396-019-0464-2. Greening, C. et al.

Gurevich, A., Saveliev, V., Vyahhi, N., Tesler, G., 2013. QUAST: quality assessment tool for genome assemblies. Bioinformatics 29, 1072–1075. https://doi.org/10.1093/bioinformatics/btt086.

Han, B., Duan, X., Wang, Y., Zhu, K., Zhang, J., Wang, R., Hu, H., Qi, F.J., Pan, J., Yan, Y., Shen, W., 2017. Methane protects against polyethylene glycol-induced osmotic stress in maize by improving sugar and ascorbic acid metabolism. Sci. Rep. 7, 46185. https://doi.org/10.1038/srep46185.

Hou, Y., Velthof, G.L., Lesschen, J.P., Staritsky, L.G., Oenama, O., 2017. Nutrient recovery and emissions of ammonia, nitrous oxide, and methane from animal manure in Europe: effects of manure treatment technologies. Environ. Sci. Technol. 51, 375–383. https://doi.org/10.1021/acs.est.6b04524.

Hou, Y., Velthof, G.L., Oenema, O., 2015. Mitigation of ammonia, nitrous oxide and methane emissions from manure management chains: a meta-analysis and integrated assessment. Glob. Chang Biol. 21, 293–1312. https://doi.org/10.1111/gcb.12767.

Huerta-Cepas, J., Forslund, K., Coelho, L.P., Szklarczyk, D., Jensen, L.J., von Mering, C., Bork, P., 2017. Fast genome-wide functional annotation through orthology assignment by eggNOG-mapper. Mol. Biol. Evol. 34, 2115–2122. https://doi.org/10.1101/076331.

Hyatt, D., Chen, G., LoCascio, P.F., Land, M.L., Larimer, F.W., Hauser, L.J., 2010. Prodigal: prokaryotic gene recognition and translation initiation site identification. BMC Bioinf. 11, 119. https://doi.org/10.1186/1471-2105-11-119.

IPCC, 2022. Impacts of 1.5°C global warming on natural and human systems. Global Warming of 1.5°C 175–312. https://www.ipcc.ch/sr15/chapter/chapter-3.

Jain, C., Rodriguez-R, L.M., Phillippy, A.M., Konstantinidis, K.T., Aluru, S., 2018. High throughput ANI analysis of 90K prokaryotic genomes reveals clear species boundaries. Nat. Commun. 9, 5114. https://doi.org/10.1038/s41467-018-07641-9.

Kamke, J., Kittelmann, S., Soni, P., Li, Y., Tavendale, M., Ganesh, S., Janssen, P.H., Shi, W.B., Froula, J., Rubin, E.M., Attwood, G.T., 2016. Rumen metagenome and metatranscriptome analyses of low methane yield sheep reveals a *Sharpea*-enriched microbiome characterised by lactic acid formation and utilisation. Microbiome 4, 56. https://doi.org/10.1186/s40168-016-0201-2.

Kang, D.D., Li, F., Kirton, E., Thomas, A., Egan, R., An, H., Wang, Z., 2019. MetaBAT 2: an adaptive binning algorithm for robust and efficient genome reconstruction from metagenome assemblies. PeerJ 7, e7359. https://doi.org/10.7717/peerj.7359.

Kruger Ben Shabat, S., Sasson, G., Doron-Faigenboim, A., Durman, T., Yaacoby, S., Miller, M.E.B., White, B.A., Shterzer, N., Mizrahi, I., 2016. Specific microbiome-dependent mechanisms underlie the energy harvest efficiency of ruminants. ISME J. 10, 2958–2972. https://doi.org/10.1038/ismej.2016.62.

Langfelder, P., Horvath, S., 2008. WGCNA: an R package for weighted correlation network analysis. BMC Bioinf. 9, 1–13. https://doi.org/10.1186/1471-2105-9-559.

Li, D., Liu, C.M., Luo, R., Sadakane, K., Lam, T., 2015. MEGAHIT: An ultra-fast single-node solution for large and complex metagenomics assembly via succinct de Bruijn graph. Bioinformatics 31, 1674–1676. https://doi.org/10.1093/bioinformatics/btv033.

Li, J., Xiao, L., Zheng, S., Zhang, Y., Luo, M., Tong, C., Xu, H., Tan, Y., Liu, J., Wang, O., Liu, F., 2018. A new insight into the strategy for methane production affected by conductive carbon cloth in wetland soil: beneficial to acetoclastic methanogenesis instead of $CO_2$ reduction. Sci. Total Environ. 643, 1024–1030. https://doi.org/10.1016/j.scitotenv.2018.06.271.

Maasakkers, J.D., Jacob, D.J., Sulprizio, M.P., Scarpelli, T.R., Nesser, H., Sheng, J.X., Zhang, Y., Hersher, M., Bloom, A.A., Bowman, K.W., Worden, J.R., Janssens-Maenhout, G., Parker, R.J., 2019. Global distribution of methane emissions, emission trends, and OH concentrations and trends inferred from an inversion of GOSAT satellite data for 2010-2015. Atmos. Chem. Phys. 19, 7859–7881. https://doi.org/10.5194/acp-19-7859-2019. Maasakkers, J. D. et al.

Mizrahi, I., Wallace, R.J., Moraïs, S., 2021. The rumen microbiome: balancing food security and environmental impacts. Nat. Rev. Microbiol. 19, 553–566. https://doi.org/10.1038/s41579-021-00543-6.

Moraïs, S., Mizrahi, I., 2019. The road not taken: the rumen microbiome, functional groups, and community states. Trends Microbiol. 27, 538–549. https://doi.org/10.1016/j.tim.2018.12.011.

Morita, M., Malvankar, N.S., Franks, A.E., Summers, Z.M., Giloteaux, L., Rotaru, A., Rotaru, C., Lovley, D.R., 2011. Potential for direct interspecies electron transfer in methanogenic wastewater digester aggregates. mBio 2. https://doi.org/10.1128/mBio.00159-11, 00159-11.

Nguyen, L.T., Schmidt, H.A., von Haeseler, A., Minh, B.Q., 2014. IQ-TREE: a fast and effective stochastic algorithm for estimating maximum-likelihood phylogenies. Mol. Biol. Evol. 32, 268–274. https://doi.org/10.1093/molbev/msu300.

Owen, J.J., Silver, W.L., 2015. Greenhouse gas emissions from dairy manure management: a review of field-based studies. Glob. Chang Biol. 21, 550–565. https://doi.org/10.1111/gcb.12687.

Patro, R., Duggal, G., Love, M.I., Lrizarry, R.A., Kingsford, C., 2017. Salmon provides fast and bias-aware quantification of transcript expression. Nat. Methods 14, 417–419. https://doi.org/10.1038/nmeth.4197.

Peng, X., 2021. Genomic and functional analyses of fungal and bacterial consortia that enable lignocellulose breakdown in goat gut microbiomes. Nat. Microbiol. 6, 499–511. https://doi.org/10.1038/s41564-020-00861-0.

Pérez-Barbería, F.J., 2017. Scaling methane emissions in ruminants and global estimates in wild populations. Sci. Total Environ. 579, 1572–1580. https://doi.org/10.1016/j.scitotenv.2016.11.175.

Poulsen, M., Schwab, C., Borg Jensen, B., Engberg, R.M., Spang, A., Canibe, N., Højberg, O., Milinovich, G., Fragner, L., Schleper, C., Weckwerth, W., Lund, P., Schramm, A., Urich, T., 2013. Methylotrophic methanogenic Thermoplasmata implicated in reduced methane emissions from bovine rumen. Nat. Commun. 4, 1428. https://doi.org/10.1038/ncomms2432.

Rotaru, A., Shrestha, P.M., Liu, F., Shrestha, M., Shrestha, D., Embree, M., Zengler, K., Wardman, C., Nevin, K.P., Lovley, D.R., 2014. A new model for electron flow during anaerobic digestion: direct interspecies electron transfer to *Methanosaeta* for the reduction of carbon dioxide to methane. Energy Environ. Sci. 7, 408–415. https://doi.org/10.1039/C3EE42189A.

Sasson, G., Kruger Ben-Shabat, S., Seroussi, E., Doron-Faigenboim, A., Shterzer, N., Yaacoby, S., Berg Miller, M.E., White, B.A., Halperin, E., Mizrahi, I., 2017. Heritable bovine rumen bacteria are phylogenetically related and correlated with the cow's capacity to harvest energy from its feed. mBio 8, e00703–e00717. https://doi.org/10.1128/mBio.00703-17.

Saunois, M., Bousquet, P., Poulter, B., Peregon, A., Ciais, P., Canadell, J.G., Dlugokencky, E.J., Etiope, G., Bastviken, D., Houweling, S., Janssens-Maenhout, G., Tubiello, F.N., Castaldi, S., Jackson, R.B., Alexe, M., Arora, V.K., Beerling, D.J., Bergamaschi, P., Blake, D.R., Brailsford, G., Brovkin, V., Bruhwiler, L., Crevoisier, C., Crill, P., Covey, K., Curry, C., Frankenberg, C., Gedney, N., Höglund-Isaksson, L., Ishizawa, M., Ito, A., Joos, F., Kim, H.-S., Kleinen, T., Krummel, P., Lamarque, J.-F., Langenfelds, R., Locatelli, R., Machida, T., Maksyutov, S., McDonald, K.C., Marshall, J., Melton, J.R., Morino, I., Naik, V., O'Doherty, S., Parmentier, F.-J.W., Patra, P.K., Peng, C., Peng, S., Peters, G.P., Pison, I., Prigent, C., Prinn, R., Ramonet, M., Riley, W.J., Saito, M., Santini, M., Schroeder, R., Simpson, I.J., Spahni, R., Steele, P., Takizawa, A., Thornton, B.F., Tian, H., Tohjima, Y., Viovy, N., Voulgarakis, A., van Weele, M., van der Werf, G.R., Weiss, R., Wiedinmyer, C., Wilton, D.J., Wiltshire, A., Worthy, D., Wunch, D., Xu, X., Yoshida, Y., Zhang, B., Zhang, Z., Zhu, Q., 2016. The global methane budget 2000-2012. Earth Syst. Sci. Data 8, 697–751. https://doi.org/10.5194/essd-8-697-2016.

Uritskiy, Gv, Diruggiero, J., Taylor, J., 2018. MetaWRAP - a flexible pipeline for genome-resolved metagenomic data analysis. Microbiome 6, 158. https://doi.org/10.1186/s40168-018-0541-1.

Vanwonterghem, I., Evans, P.N., Parks, D.H., Jensen, P.D., Woodcroft, B.J., Hugenholtz, P.B., Tyson, G.W., 2016. Methylotrophic methanogenesis discovered in the archaeal phylum Verstraetearchaeota. Nat. Microbiol. 1, 16170. https://doi.org/10.1038/NMICROBIOL.2016.170.

Wallace, R.J., Sasson, G., Garnsworthy, P.C., Tapio, I., Gregson, E., Bani, P., Huhtanen, P., Bayat, A.R., Strozzi, F., Biscarini, F., Snelling, T.J., Saunders, N., Potterton, S.L., Craigon, J., Minuti, A., Trevisi, E., Callegari, M.L., Cappelli, F.P., Cabezas-Garcia, E.H., Vilkki, J., Pinares-Patiño, C.S., Fliegerová, K.O., Mrázek, J., Sechovcová, H., Kopečný, J., Bonin, A., Boyer, F., Taberlet, P., Kokou, F., Halperin, E., Williams, J.L., Shingfield, K.J., Mizrahi, I., 2019. A heritable subset of the core rumen microbiome dictates dairy cow productivity and emissions. Sci. Adv. 5, eaav8391. https://doi.org/10.1126/sciadv.aav8391.

Wegener, G., Krukenberg, V., Riedel, D., Tagetmeyer, H.E., Boetius, A., 2015. Intercellular wiring enables electron transfer between methanotrophic archaea and bacteria. Nature 526, 587–590. https://doi.org/10.1038/nature15733.

Wood, D.E., Lu, J., Langmead, B., 2019. Improved metagenomic analysis with Kraken 2. Genome Biol. 20, 257. https://doi.org/10.1186/s13059-019-1891-0.

Woodcroft, B.J., Singleton, C.M., Boyd, J.A., Evans, P.N., Emerson, J.B., Zayed, A.A.F., Hoelzle, R.D., Lamberton, T.O., McCalley, C.K., Hodgkins, S.B., Wilson, R.M., Purvine, S.O., Nicora, C.D., Li, C., Frolking, S., Chanton, J.P., Crill, P.M., Saleska, S. R., Rich, V.I., Tyson, G.W., 2018. Genome-centric view of carbon processing in thawing permafrost. Nature 560, 49–54. https://doi.org/10.1038/s41586-018-0338-1.

Wu, Y.-W., Simmons, B.A., Singer, S.W., 2016. MaxBin 2.0: an automated binning algorithm to recover genomes from multiple metagenomic datasets. Bioinformatics 32, 605–607. https://doi.org/10.1093/bioinformatics/btv638.

Xiao, L., Liu, F., Lichtfouse, E., Zhang, P., Feng, D., Li, F., 2020a. Methane production by acetate dismutation stimulated by *Shewanella oneidensis* and carbon materials: an alternative to classical $CO_2$ reduction. Chem. Eng. J. 389, e124469. https://doi.org/10.1016/j.cej.2020.124469.

Xiao, L., Liu, F., Liu, J., Li, J., Zhang, Y., Yu, J., Wang, O., 2018. Nano-$Fe_3O_4$ particles accelerating electromethanogenesis on an hour-long timescale in wetland soil. Environ. Sci.: Nano 5, 436–445. https://doi.org/10.1039/C7EN00577F.

Xiao, L., Sun, R., Zhang, P., Zheng, S., Tan, Y., Li, J., Zhang, Y., Liu, F., 2019. Simultaneous intensification of direct acetate cleavage and $CO_2$ reduction to generate methane by bioaugmentation and increased electron transfer. Chem. Eng. J. 378, 3022–3027. https://doi.org/10.1016/j.cej.2019.122229.

Xiao, L., Zheng, S., Lichtfouse, E., Luo, M., Tan, Y., Liu, F., 2020b. Carbon nanotubes accelerate acetoclastic methanogenesis: from pure cultures to anaerobic soils. Soil Biol. Biochem. 150, e107938. https://doi.org/10.1016/j.soilbio.2020.107938.

Yu, J., Liu, J., Senthil Kumar, P., Wei, Y., Zhou, M., Vo, D.N., Xiao, L., 2022. Promotion of methane production by magnetite via increasing acetogenesis revealed by metagenome-assembled genomes. Bioresour. Technol. 345, e126521. https://www.x-mol.com/paperRedirect/1469014804960681984.

Zhang, H., Yohe, T., Huang, L., Entwistle, S., Wu, P., Yang, Z., Busk, P.K., Xu, Y., Yin, Y., 2018. dbCAN2: a meta server for automated carbohydrate-active enzyme annotation. Nucleic Acids Res. 46, W95. https://doi.org/10.1093/nar/gky418.

Zhang, Q.Q., Difford, G., Sahana, G., Lovendahl, P., Lassen, J., Lund, M.S., Guldbrandtden, B., Janss, L., 2020. Bayesian modeling reveals host genetics associated with rumen microbiota jointly influence methane emission in dairy cows. ISME J. 14, 2019–2033. https://doi.org/10.1038/s41396-020-0663-x.

Zhou, M., Hernandez-Sanabria, E., Le, L.G., 2009. Assessment of the microbial ecology of ruminal methanogens in cattle with different feed efficiencies. Appl. Environ. Microbiol. 75, 6524–6533. https://doi.org/10.1128/AEM.02815-08.